Premature endocycling of *Drosophila* follicle cells causes pleiotropic defects in oogenesis

Hunter C. Herriage[1] and Brian R. Calvi[1,2]

1: Department of Biology, Indiana University, Bloomington, IN 47405

2: Corresponding author, bcalvi@indiana.edu

Keywords: endocycling, border cells, polyploidy, oogenesis, epithelium, *Drosophila*

Summary Statement

A premature switch to polyploid endocycles in *Drosophila* ovarian follicle cells caused pleiotropic defects in oogenesis and compromised female fertility, revealing new ways in which unscheduled endocycles cause developmental defects.

Abstract

Endocycling cells grow and repeatedly duplicate their genome without dividing. Cells switch from mitotic cycles to endocycles in response to developmental signals during the growth of specific tissues in a wide range of organisms. The purpose of switching to endocycles, however, remains unclear in many tissues. Additionally, cells can switch to endocycles in response to conditional signals, which can have beneficial or pathological effects on tissues. However, the impact of these unscheduled endocycles on development is underexplored. Here, we use *Drosophila* ovarian somatic follicle cells as a model to examine the impact of unscheduled endocycles on tissue growth and function. Follicle cells normally switch to endocycles at mid-oogenesis. Inducing follicle cells to prematurely switch to endocycles resulted in lethality of the resulting embryos. Analysis of ovaries with premature follicle cell endocycles revealed aberrant follicular epithelial structure and pleiotropic defects in oocyte growth, developmental gene amplification, and the migration of a special set of follicle cells known as border cells. Overall, these findings reveal how unscheduled endocycles can disrupt tissue growth and function to cause aberrant development.

Introduction

Many tissues grow via a variant cell cycle known as the endocycle. Endocycles are characterized by alternating G and S phases without mitotic division, resulting in the growth of large polyploid cells (Calvi, 2013). A regulated switch from mitotic cycles to endocycles is part of normal developmental growth programs of specific tissues across *Eukarya* (Fox and Duronio, 2013; Ovrebo and Edgar, 2018; Shu et al., 2018). In contrast, cells can also switch to unscheduled endocycles in response to stress and other conditional signals (Bailey et al., 2021; Hassel et al., 2014; Qi and Calvi, 2016; Rotelli et al., 2019). These induced endocycling cells can be beneficial for wound healing and regeneration, but they can also have pathological effects, including the promotion of cancer (Bailey et al., 2021; Herriage et al., 2023; Pienta et al., 2022; Shu et al., 2018). Much remains unknown, however, about how unscheduled endocycling affects tissue structure and function.

In this study we use the somatic follicle cells of the *Drosophila* ovary as a model to evaluate the effects of unscheduled endocycles on tissue function. A *Drosophila* ovary consists of ~16 ovarioles, each composed of one germarium stem cell compartment followed by an “assembly line” of progressively developing egg chambers in 14 stages of oogenesis (Fig. 1A) (Duhart et al., 2017; King, 1970). These developing egg chambers contain the germline (15 endocycling nurse cells and one oocyte) ensheathed by an epithelium of somatic follicle cells (Fig. 1A) (Jia et al., 2015; King, 1970). Follicle cells originate from a population of two to four somatic stem cells in the germarium and proliferate mitotically over the course of three days until stage 6 of oogenesis (Fadiga and Nystul, 2019; Margolis and Spradling, 1995; Sun and Deng, 2007). In response to Notch signaling at stages 6 / 7, follicle cells switch to the endocycle and subsequently complete three genome duplications over the next ~24 hours (Fig. 1A) (Calvi et al., 1998; Deng et al., 2001; Lopez-Schier and St Johnston, 2001; Spradling, 1993). After achieving a DNA copy number (C) of 16C, follicle cells arrest endocycles at different times (asynchronously) during late stage 9. Follicle cells then synchronously initiate a specialized DNA rereplication program in stage 10B that selectively amplifies the DNA copy number of eggshell (chorion) protein genes, a process known as chorion gene amplification (Fig. 1A) (Calvi et al., 1998; Spradling and Mahowald, 1980). Disruption of this process causes thin eggshells and embryonic lethality (Calvi, 2006; Spradling and Mahowald, 1980). Follicle cells also support egg growth by mediating transport of yolk proteins into the oocyte and

64 participate in patterning of the egg and embryo (Brennan et al., 1982; Duhart et al., 2017;
65 Merkle et al., 2020; Raikhel and Dhadialla, 1992). While it is known that follicle cells have
66 these important roles in oogenesis, it remains unclear what biological function is served by the
67 endocycle switch occurring specifically at stage 6. In this study, we find that unscheduled
68 endocycles can have severe negative consequences, with broader impacts on understanding
69 how they may contribute to human disease.
70

71 **Results and Discussion**

72 Induction of premature endocycles in follicle cells

73 To address whether a switch to follicle cell endocycles before stage 6 would affect
74 oogenesis, we induced premature endocycling by expressing the protein Roughex (Rux), a
75 repressor of Cyclin A / CDK1 activity and mitotic entry (Avedisov et al., 2000; Sprenger et al.,
76 1997). A *tj-GAL4* transgene induced expression of a *UAS-Rux* transgene in all ovarian somatic
77 cells, and a temperature-sensitive GAL80^{ts} repressor of GAL4 permitted control over timing of
78 expression (Brand and Perrimon, 1993; McGuire et al., 2004; Weaver et al., 2020). The *tj-*
79 *GAL4 tub-GAL80^{ts} / UAS-Rux* experimental and *tj-GAL4 tub-GAL80^{ts} /* + control animals were
80 raised at 18°C to repress GAL4 activity. Adult flies were then shifted to 29°C to induce *UAS-*
81 *Rux* expression and ovaries were examined one and two days thereafter (Fig. 1A). Within one
82 day after *UAS-Rux* expression, stage 1-6 follicle cells ceased labeling for the mitotic marker
83 phosphorylated Histone H3 (pH3) but continued to incorporate the nucleotide analog 5-ethynyl
84 2′-deoxyuridine (EdU), suggesting that they had switched to G / S endocycles (Fig. S1A-D′).

85 We next asked what effect premature endocycle induction would have on follicle cells as
86 they matured to later stages of oogenesis (Fig. 1A). Two days after a shift to 29°C, stage 10B
87 egg chambers from control females had a normal ~641 follicle cells, and measurement of DAPI
88 fluorescence indicated that they had the normal DNA content of ~16C (Fig. 1A-B′, D, E) (Calvi
89 et al., 1998; Sun and Deng, 2007). In contrast, induction of premature endocycles two days
90 earlier resulted in stage 10B egg chambers with four-fold fewer follicle cells (~179) and nearly
91 a four-fold increase in average DNA content (mean ploidy ~56 C) (Fig. 1C-E). Immunolabeling
92 for E-cadherin also indicated that these stage 10B follicle cells were larger than normal,
93 consistent with the known scaling of cell size with DNA ploidy (Fig. 1B′, C′) (Cadart and Heald,
94 2022; Tepass et al., 1996; Uemura et al., 1996). These results suggest that Rux-expressing
95 follicle cells had skipped two mitotic divisions and instead underwent two extra endocycle

genome doublings. These results are consistent with the known rate of oogenesis at 29°C (Gandara and Drummond-Barbosa, 2022). These stage 10B egg chambers would have been in approximately stage 4 / 5 two days earlier at the time of temperature shift (Gandara and Drummond-Barbosa, 2022). Normally, follicle cells in a stage 4 / 5 egg chamber undergo an average of two mitotic divisions over one day as it matures to stage 6 / 7, after which follicle cells endocycle over the next day from stage 7 to stage 10A (Calvi et al., 1998; Margolis and Spradling, 1995). Given that there were two extra genome doublings instead of the normal two mitotic divisions during the ~24 hours from stage 4 / 5 to stage 6 / 7, these data also suggest that the duration of each induced endocycle is approximately equal to that of the mitotic cycles that they supplanted (Margolis and Spradling, 1995). Moreover, the increased DNA content of these follicle cells at stage 10 suggests that starting endocycles early can override the undefined cell-autonomous mechanisms that arrest endocycles to limit follicle cell ploidy to 16C.

<u>Premature endocycling has deleterious effects on oogenesis and female fertility</u>

We next examined whether premature follicle cell endocycles affected the morphology of late-stage egg chambers. Stage 10B egg chambers from Rux-expressing females appeared similar to those from controls (Fig 1B-C'). The main body follicle cells underwent normal migration posteriorly during stage 9 to over the growing oocyte (Figs. 1B-C', 2A-D). Measurements indicated that one day after temperature shift, stage 10B egg chambers from Rux-expressing females had oocytes of a similar size to controls (Fig. 2A- E). These egg chambers would have been in approximately stage 6 / 7 one day earlier at the time of temperature shift, a stage when follicle cells normally enter endocycles, and, therefore, would have begun endocycling no more than a few hours early. Conversely, two days after temperature shift, the Rux-expressing stage 10B egg chambers that had begun endocycles in stage 4 / 5 had oocytes that were smaller than controls (Fig. 2C-E). Correspondingly, the length of the nurse cell compartment in these stage 10B egg chambers was larger than controls after two days of Rux expression (Fig. 2F). These results suggest that the two extra follicle cell endocycles had non-autonomous effects on germline growth, which may include the function of follicle cells to mediate oocyte yolk deposition (Brennan et al., 1982; Horne-Badovinac and Bilder, 2005; Isasti-Sanchez et al., 2021; Raikhel and Dhadialla, 1992).

127 Another important function of follicle cells is to synthesize the eggshell late in
128 oogenesis, a process that is supported by chorion gene amplification (Fig. 1A) (Calvi et al.,
129 1998; Spradling and Mahowald, 1980). This selective gene amplification can be detected as
130 distinct foci of EdU incorporation beginning in stage 10B (Calvi et al., 1998). EdU labeling of *tj-*
131 *GAL4 GAL80*^{ts} / + control ovaries at 29°C showed that all follicle cells over the oocyte had
132 nuclear foci of EdU at the onset of stage 10B, indicating that the onset of amplification was
133 synchronized among follicle cells, as previously described (Fig. 2G, I-I′, K) (Calvi et al., 1998).
134 Follicle cells that had been expressing Rux for 24 hours also had the normal transition to
135 synchronous amplification in stage 10B (Fig. 2H). In contrast, induction of premature
136 endocycles two days earlier resulted in some stage 10B egg chambers with a mixture of follicle
137 cells that had either the normal amplification foci or pan-nuclear EdU incorporation indicative of
138 continued genomic replication (Fig. 2J-K). These results suggest that a premature start to
139 endocycles in earlier oogenesis disrupts the normal cessation of endocycles and the
140 synchronous initiation of amplification in later oogenesis. Further analyses of these induced
141 endocycles may provide insight into the mechanisms that coordinate the transition from
142 endocycles to amplification during stage 10, which may be similar to the mechanisms that
143 govern endocycle arrest and determine final DNA content in other polyploid cell types.
144 Defects in chorion gene amplification are known to result in thin eggshells and reduced
145 embryo viability (Calvi, 2006). We therefore examined whether premature endocycles impaired
146 eggshell synthesis. Females expressing *UAS-Rux* began laying eggs with thin shells one day
147 after induction, a phenotype that greatly increased in frequency after two days (Fig. 2L-P, Fig.
148 S2A, B). Expression of Rux in females also resulted in reduced viability of their embryos, as
149 evidenced by a reduction in egg hatching beginning on day one, which was further reduced on
150 days two and three (Fig. 2Q). Three or more days of Rux expression resulted in ovarioles with
151 degenerating stage 8-9 egg chambers, diagnostic of an ovarian stress response known as the
152 vitellogenic checkpoint (Fig. S2 C, D) (Peterson et al., 2015; Serizier and McCall, 2017). This
153 result suggests that very early entry into endocycles in stage 1 / 2 triggers a general stress
154 response three days later in stage 8. All together, these data indicate that induction of
155 premature follicle cell endocycles has deleterious effects on egg quality and female fertility.
156
157
158

159 Premature endocycles cause structural defects in the follicular epithelium

160 After Rux expression, there was a one to several day delay in later oogenesis defects
161 and reduced embryo viability. This delay suggested that these defects were the manifestation
162 of premature endocycle entry at earlier stages. To examine the structure of the follicular
163 epithelium in early stage egg chambers, we immunolabeled for the cell-cell junction protein E-
164 cadherin (Godt and Tepass, 1998; Oda et al., 1997; Tepass et al., 1996; Uemura et al., 1996).
165 Although EdU and pH3 labeling had indicated that follicle cells switch to endocycles within one
166 day of Rux expression, this duration of induced endocycling did not cause major defects in
167 epithelial structure (Figs. S1A-B′, 3A-B″). These follicle cells had a uniform, cuboidal structure
168 and E-cadherin labeling on their apical surface that is adjacent to the germline (Fig. 3A-B″)
169 (Godt and Tepass, 1998; Gonzalez-Reyes and St Johnston, 1998). In contrast, after two days
170 of Rux expression, follicle cells were all larger with wide variations in their size and shape
171 within an egg chamber (Fig. 3C-D″). Some follicle cells had highly irregular shapes, with
172 different parts of the cell having unequal thicknesses in the apical / basal axis, and many with
173 highly irregular E-cadherin labeling (Fig. 3D-D″). In confocal sections through the middle of egg
174 chambers, the interface between the follicular epithelium and germline appeared wavy instead
175 of the normal smooth circular interface, suggesting global deformations of tissue morphology
176 (Fig. 3C′, D′). Labeling for the membrane-associated protein Discs large 1 (Dlg1) also revealed
177 irregular cell sizes and shapes, but Dlg1 had an overall normal basolateral localization,
178 suggesting that there was not a severe disruption of cell polarity (Fig. S3A-D″) (Khoury and
179 Bilder, 2020; Woods et al., 1996). All follicle cells in these aberrant egg chambers had an
180 increased DNA content consistent with having proceeded through premature endocycles (Fig.
181 3C-E).

182 These disruptions of epithelial structure in early stages may contribute to the observed
183 defects in later stages of oogenesis over subsequent days. This includes the reduction in
184 oocyte growth in stage 10 egg chambers, which is mediated by a paracelluar transport of yolk
185 protein across the follicular epithelium beginning in stage 8 (Isasti-Sanchez et al., 2021;
186 Riechmann, 2021). This regulated permeability of the epithelium is known as patency, and is
187 mediated by remodeling of cell-cell junctions through a mechanism that includes E-cadherin
188 (Isasti-Sanchez et al., 2021). Thus, the aberrant E-cadherin labeling and cell and epithelial
189 morphology we observe in induced endocycling cells may disturb the remodeling of cell-cell
190 contacts that is required for patency and oocyte growth. More broadly, these results suggest

that disrupted epithelial structure and permeability in other tissues may be another way for unscheduled endocycles to contribute to disease.

Premature endocycling inhibits border cell migration

Unlike the main body follicle cells that migrate on the surface of the egg chamber, another group of follicle cells delaminate from the anterior epithelium and migrate posteriorly between the nurse cells during stage 9 (Mishra et al., 2019; Montell et al., 1992; Montell et al., 2012; Spradling, 1993). This collective migration event is initiated in early stage 9 when two specialized follicle cells, known as the polar cells, recruit 4-6 neighboring follicle cells to become border cells via JAK-STAT signaling (Montell et al., 1992; Silver and Montell, 2001). After arriving at their final destination at the anterior of the growing oocyte in stage 10A, this migrating border cell cluster forms the sperm entry port known as the micropyle (Bishop and King, 1984; King, 1970). Because these border cells are a powerful model for mechanisms of collective cell migration during metastasis, we wished to investigate the effect of premature endocycling on their migration.

We identified border cells based on their elevated E-cadherin levels in control and Rux-expressing ovaries two days after induction at 29°C and measured the distance they had migrated relative to main body follicle cells in the same egg chamber during stage 9-10A (Niewiadomska et al., 1999; Oda et al., 1997). In controls, the migration of the border cell cluster between the nurse cells stayed on-pace with the anterior of the main body follicle cells that are migrating on the surface of the egg chamber during stage 9, with both populations of follicle cells reaching the oocyte at the onset of stage 10A (Fig. 4A, A', C). In contrast, Rux expression resulted in border cells lagging behind the main body follicle cells to varying extents (Fig. 4B-C). In some egg chambers, border cells had failed to even delaminate from the epithelium at the anterior pole of the egg chamber by stage 10 (Fig. 4C). Having abnormal numbers of polar cells or border cells can inhibit border cell cluster delamination and migration (Silver et al., 2005; Silver and Montell, 2001). Labeling for the polar cell marker protein Fasciclin III (Fas III) showed that after two days of Rux expression egg chambers had the normal two polar cells, including those in which border cells migrated slowly or failed to delaminate from the epithelium (Fig. 4D-E‴) (Ruohola et al., 1991). Co-labeling against E-cadherin indicated that these migrating clusters had normal structure and cell polarity (Fig. 4D-E‴). While some Rux-expressing egg chambers had a reduced number of cells per cluster,

223 even clusters composed of the normal number of cells were delayed in their migration (Fig. 4B,
224 B′, E-E‴). Our observation of impaired collective border cell migration contrasts with recent
225 evidence that polyploidy enhances migration of cancer cells *in vitro,* and suggestions that it
226 promotes collective cell migration during metastasis (Godinho et al., 2014; Mallin et al., 2023;
227 Wang et al., 2019). Our results raise the possibility that the effects of unscheduled endocycles
228 on cell migration are dependent on cell type and tissue context (Lamb et al., 2021; Penfield
229 and Montell, 2023). In addition, oncogenic mutations may synergize with the polyploid state to
230 give rise to emergent migratory properties (Almeida Machado Costa et al., 2022).
231
232 Conclusions
233 Overall, our findings show that unscheduled endocycles can have severe pleiotropic
234 effects on epithelial structure and function. Further characterization of these effects will lead to
235 a greater understanding of the different ways in which unscheduled endocycling can impact
236 development and contribute to disease.
237

238 **Materials and Methods**

239 *Drosophila* genetics: Crosses of *tj-GAL4 tub-GAL80^{ts} / CyO* to *w^{1118}* (control) or *UAS-Rux /*
240 *SM6a* (experimental) were conducted, and their offspring were reared, at 18°C during larval
241 and early adult development. The resulting adult female offspring were fed wet yeast with
242 males for 2 days at 18°C before being transferred to new wet yeast and shifted to 29°C for 1,
243 2, or 3 days (as noted in the text). The females and males were transferred to new wet yeast
244 every 2 days during the experiments. The *tj-GAL4, tub-GAL80^{ts}* / *CyO* strain was a generous
245 gift from L. Weaver. The *UAS-Rux / SM6a* strain was obtained from the Bloomington
246 Drosophila Stock Center (BDSC #9166).

247 Immunofluorescence microscopy: Ovaries were fixed and labeled as previously described
248 (Schwed et al., 2002). For E-cadherin labeling, fixation buffers were supplemented with 1 mM
249 $CaCl_2$. The following antibodies and dilutions were used: rat anti-shg (fly E-cadherin), 1:20
250 (DSHB DCAD2); rabbit anti-phosphorylated histone H3 (pH3), 1:1000 (Millipore 06-570);
251 mouse anti-Dlg1, 1:200 (DSHB 4F3); mouse anti-FasIII, 1:50 (DSHB 7G10). EdU incorporation
252 *in vitro* was for 1 hour as previously described (Calvi and Lilly, 2004). Asynchronous chorion
253 gene amplification was defined by stage 10B egg chambers with both punctate and pan-
254 nuclear EdU labeling of follicle cell nuclei. Egg chambers with more than one pan-nuclear EdU
255 labeled nucleus were scored as "asynchronous." Fluorescence micrographs were taken on a
256 Leica SP8 confocal. DIC images of stage 10B egg chambers were taken using a Leica
257 DM5500 B. Brightfield images of laid eggs were taken using a Zeiss SteREO Discovery.V12.
258 Nuclear DNA content was quantified using ImageJ/FIJI by measuring mean DAPI fluorescence
259 per pixel in a nucleus, subtracting local mean background DAPI fluorescence per pixel, and
260 then multiplying the difference by the number of pixels per nucleus to obtain the corrected total
261 DAPI fluorescence intensity. The number of follicle cells, oocyte area, nurse cell compartment
262 length, and border cell migration were quantified using ImageJ/FIJI.

263 Eggshell scoring and egg hatch rate: Eggs from well-fed and mated females were collected on
264 grape plates with a thin layer of yeast paste for 2-4 hours for each respective day of 29°C
265 transgene induction. After counting the number of eggs with thin eggshells, eggs were lined up
266 and incubated at 18°C to ensure no GAL4-driven transgene expression affected their viability.
267 They were then scored for hatching over four subsequent days.

268 Statistical Analysis: Data graphing and statistical analyses were carried out in GraphPad
269 Prism. Data were tested for normality and homoscedasticity to determine correct analyses.
270 Sample size (n) is defined as the total of independent observations / measurements used for
271 the chosen analysis across multiple biological replicates. All averages shown are mean ± s.d.,
272 except for Figure 2K, which is mean ± s.e.m. Two-tailed Mann-Whitney tests were used to test
273 for significance in Figs. 1D, 2E, and 3E. Fig. 2E was corrected for multiple comparisons. A two-
274 tailed unpaired Welch's t-test was used to test for significance in Fig. 1E. A Mixed Effects Two-
275 Way ANOVA was used to test for significance in Fig. 2F. A two-tailed unpaired t-test was used
276 to test for significance in Fig. 2K.

277

Acknowledgements

We thank S. Brown and Y.T. Huang for experimental assistance. We are appreciative of the thoughtful feedback on the research and manuscript from S. Brown, L. Hesting, Y.T. Huang, P. Rangarajan, and C. Walczak. We thank A. Kun and J. Powers of the IU Light Microscopy Imaging Center, supported in part by the Office of the Vice Provost of Research. Special thanks to L. Weaver for her generous gift of the *tj-GAL4 tub-GAL80^{ts} / CyO* strain.

Competing Interests

The authors declare no competing interests.

Author Contributions

H.C.H. performed experiments and statistical analyses. Both authors wrote and edited the manuscript. B.R.C. secured funding and provided mentorship and supervision.

Funding

This work was supported by National Institutes of Health Grant NIH R01GM113107 to B.R.C.

References

Almeida Machado Costa, C., Wang, X. F., Ellsworth, C. and Deng, W. M. (2022). Polyploidy in development and tumor models in Drosophila. *Semin Cancer Biol* **81**, 106-118.

Avedisov, S. N., Krasnoselskaya, I., Mortin, M. and Thomas, B. J. (2000). Roughex mediates G(1) arrest through a physical association with cyclin A. *Mol Cell Biol* **20**, 8220-8229.

Bailey, E. C., Kobielski, S., Park, J. and Losick, V. P. (2021). Polyploidy in Tissue Repair and Regeneration. *Cold Spring Harb Perspect Biol* **13**.

Bishop, D. L. and King, R. C. (1984). An ultrastructural study of ovarian development in the otu-7 mutant of Drosophila melanogaster. *J. Cell Sci.* **67**, 87-119.

Brand, A. and Perrimon, N. (1993). Targeted gene expression as a means of altering cell fates and generating dominant phenotypes. *Development* **118**, 401-415.

Brennan, M. D., Weiner, A. J., Goralski, T. J. and Mahowald, A. P. (1982). The follicle cells are a major site of vitellogenin synthesis in Drosophila melanogaster. *Dev Biol* **89**, 225-236.

Cadart, C. and Heald, R. (2022). Scaling of biosynthesis and metabolism with cell size. *Molecular Biology of the Cell* **33**, pe5.

Calvi, B. R. (2006). Developmental DNA amplification. In *DNA replication and human disease* (ed. M. L. DePamphilis), pp. 233-255. Cold Spring Harbor, NY: Cold Spring Harbor Laboratory Press.

Calvi, B. R. (2013). Making big cells: one size does not fit all. *Proc Natl Acad Sci U S A* **110**, 9621-9622.

Calvi, B. R., Lilly, M. A. and Spradling, A. C. (1998). Cell cycle control of chorion gene amplification. *Genes Dev* **12**, 734-744.

Deng, W. M., Althauser, C. and Ruohola-Baker, H. (2001). Notch-Delta signaling induces a transition from mitotic cell cycle to endocycle in Drosophila follicle cells. *Development* **128**, 4737-4746.

Duhart, J. C., Parsons, T. T. and Raftery, L. A. (2017). The repertoire of epithelial morphogenesis on display: Progressive elaboration of Drosophila egg structure. *Mech Dev* **148**, 18-39.

Fadiga, J. and Nystul, T. G. (2019). The follicle epithelium in the Drosophila ovary is maintained by a small number of stem cells. *Elife* **8**.

Fox, D. T. and Duronio, R. J. (2013). Endoreplication and polyploidy: insights into development and disease. *Development* **140**, 3-12.

Gandara, A. C. P. and Drummond-Barbosa, D. (2022). Warm and cold temperatures have distinct germline stem cell lineage effects during Drosophila oogenesis. *Development* **149**.

Godinho, S. A., Picone, R., Burute, M., Dagher, R., Su, Y., Leung, C. T., Polyak, K., Brugge, J. S., Thery, M. and Pellman, D. (2014). Oncogene-like induction of cellular invasion from centrosome amplification. *Nature* **510**, 167-171.

Godt, D. and Tepass, U. (1998). Drosophila oocyte localization is mediated by differential cadherin-based adhesion. *Nature* **395**, 387-391.

Gonzalez-Reyes, A. and St Johnston, D. (1998). The Drosophila AP axis is polarised by the cadherin-mediated positioning of the oocyte. *Development* **125**, 3635-3644.

Hassel, C., Zhang, B., Dixon, M. and Calvi, B. R. (2014). Induction of endocycles represses apoptosis independently of differentiation and predisposes cells to genome instability. *Development* **141**, 112-123.

Herriage, H. C., Huang, Y. T. and Calvi, B. R. (2023). The antagonistic relationship between apoptosis and polyploidy in development and cancer. *Semin Cell Dev Biol*.

Horne-Badovinac, S. and Bilder, D. (2005). Mass transit: epithelial morphogenesis in the Drosophila egg chamber. *Dev Dyn* **232**, 559-574.

Isasti-Sanchez, J., Munz-Zeise, F., Lancino, M. and Luschnig, S. (2021). Transient opening of tricellular vertices controls paracellular transport through the follicle epithelium during Drosophila oogenesis. *Dev Cell* **56**, 1083-1099 e1085.

Jia, D., Huang, Y. C. and Deng, W. M. (2015). Analysis of Cell Cycle Switches in Drosophila Oogenesis. *Methods Mol Biol* **1328**, 207-216.

Khoury, M. J. and Bilder, D. (2020). Distinct activities of Scrib module proteins organize epithelial polarity. *Proc Natl Acad Sci U S A* **117**, 11531-11540.

King, R. C. (1970). *Ovarian Development in Drosophila melanogaster*. New York: Academic Press.

Lamb, M. C., Kaluarachchi, C. P., Lansakara, T. I., Mellentine, S. Q., Lan, Y., Tivanski, A. V. and Tootle, T. L. (2021). Fascin limits Myosin activity within Drosophila border cells to control substrate stiffness and promote migration. *Elife* **10**.

Lopez-Schier, H. and St Johnston, D. (2001). Delta signaling from the germ line controls the proliferation and differentiation of the somatic follicle cells during Drosophila oogenesis. *Genes Dev* **15**, 1393-1405.

Mallin, M. M., Kim, N., Choudhury, M. I., Lee, S. J., An, S. S., Sun, S. X., Konstantopoulos, K., Pienta, K. J. and Amend, S. R. (2023). Cells in the polyaneuploid cancer cell (PACC) state have increased metastatic potential. *Clin Exp Metastasis* **40**, 321-338.

Margolis, J. and Spradling, A. (1995). Identification and behavior of epithelial stem cells in the Drosophila ovary. *Development* **121**, 3797-3807.

McGuire, S. E., Mao, Z. and Davis, R. L. (2004). Spatiotemporal gene expression targeting with the TARGET and gene-switch systems in Drosophila. *Sci STKE* **2004**, pl6.

Merkle, J. A., Wittes, J. and Schupbach, T. (2020). Signaling between somatic follicle cells and the germline patterns the egg and embryo of Drosophila. *Curr Top Dev Biol* **140**, 55-86.

Mishra, A. K., Campanale, J. P., Mondo, J. A. and Montell, D. J. (2019). Cell interactions in collective cell migration. *Development* **146**.

Montell, D. J., Rorth, P. and Spradling, A. C. (1992). slow border cells, a locus required for a developmentally regulated cell migration during oogenesis, encodes Drosophila C/EBP. *Cell* **71**, 51-62.

Montell, D. J., Yoon, W. H. and Starz-Gaiano, M. (2012). Group choreography: mechanisms orchestrating the collective movement of border cells. *Nat Rev Mol Cell Biol* **13**, 631-645.

Niewiadomska, P., Godt, D. and Tepass, U. (1999). DE-Cadherin is required for intercellular motility during Drosophila oogenesis. *J Cell Biol* **144**, 533-547.

Oda, H., Uemura, T. and Takeichi, M. (1997). Phenotypic analysis of null mutants for DE-cadherin and Armadillo in Drosophila ovaries reveals distinct aspects of their functions in cell adhesion and cytoskeletal organization. *Genes Cells* **2**, 29-40.

Ovrebo, J. I. and Edgar, B. A. (2018). Polyploidy in tissue homeostasis and regeneration. *Development* **145**.

Penfield, L. and Montell, D. J. (2023). Nuclear lamin facilitates collective border cell invasion into confined spaces in vivo. *J Cell Biol* **222**.

Peterson, J. S., Timmons, A. K., Mondragon, A. A. and McCall, K. (2015). The End of the Beginning: Cell Death in the Germline. *Curr Top Dev Biol* **114**, 93-119.

Pienta, K. J., Hammarlund, E. U., Austin, R. H., Axelrod, R., Brown, J. S. and Amend, S. R. (2022). Cancer cells employ an evolutionarily conserved polyploidization program to resist therapy. *Semin Cancer Biol* **81**, 145-159.

Qi, S. and Calvi, B. R. (2016). Different cell cycle modifications repress apoptosis at different steps independent of developmental signaling in Drosophila. *Mol Biol Cell* **27**, 1885-1897.

Raikhel, A. S. and Dhadialla, T. S. (1992). Accumulation of yolk proteins in insect oocytes. *Annu Rev Entomol* **37**, 217-251.

Riechmann, V. (2021). Paracellular transport: Opening the gates for growth. *Dev Cell* **56**, 1075-1077.

Rotelli, M. D., Policastro, R. A., Bolling, A. M., Killion, A. W., Weinberg, A. J., Dixon, M. J., Zentner, G. E., Walczak, C. E., Lilly, M. A. and Calvi, B. R. (2019). A Cyclin A-Myb-MuvB-Aurora B network regulates the choice between mitotic cycles and polyploid endoreplication cycles. *PLoS Genet* **15**, e1008253.

Ruohola, H., Bremer, K., Baker, D., Swedlow, J., Jan, L. and Jan, Y. (1991). Role of neurogenic genes in establishment of follicle cell fate and oocyte polarity during oogenesis in Drosophila. *Cell* **66**, 433-449.

Schwed, G., May, N., Pechersky, Y. and Calvi, B. R. (2002). Drosophila minichromosome maintenance 6 is required for chorion gene amplification and genomic replication. *Mol Biol Cell* **13**, 607-620.

Serizier, S. B. and McCall, K. (2017). Scrambled Eggs: Apoptotic Cell Clearance by Non-Professional Phagocytes in the Drosophila Ovary. *Front Immunol* **8**, 1642.

Shu, Z., Row, S. and Deng, W. M. (2018). Endoreplication: The Good, the Bad, and the Ugly. *Trends Cell Biol* **28**, 465-474.

Silver, D. L., Geisbrecht, E. R. and Montell, D. J. (2005). Requirement for JAK/STAT signaling throughout border cell migration in Drosophila. *Development* **132**, 3483-3492.

Silver, D. L. and Montell, D. J. (2001). Paracrine signaling through the JAK/STAT pathway activates invasive behavior of ovarian epithelial cells in Drosophila. *Cell* **107**, 831-841.

Spradling, A. and Mahowald, A. (1980). Amplification of genes for chorion proteins during oogenesis in Drosophila melanogaster. *Proc Natl Acad Sci U S A* **77**, 1096-1100.

Spradling, A. C. (1993). Developmental Genetics of Oogenesis. In *The Development of Drosophila melanogaster* (ed. M. B. a. A. Martinez-Arias). Cold Spring Harbor, New York: Cold Spring Harbor Press.

Sprenger, F., Yakubovich, N. and O'Farrell, P. H. (1997). S-phase function of Drosophila cyclin A and its downregulation in G1 phase. *Curr Biol* **7**, 488-499.

Sun, J. and Deng, W. M. (2007). Hindsight mediates the role of notch in suppressing hedgehog signaling and cell proliferation. *Dev Cell* **12**, 431-442.

Tepass, U., Gruszynski-DeFeo, E., Haag, T. A., Omatyar, L., Torok, T. and Hartenstein, V. (1996). shotgun encodes Drosophila E-cadherin and is preferentially required during cell rearrangement in the neurectoderm and other morphogenetically active epithelia. *Genes Dev* **10**, 672-685.

429 **Uemura, T., Oda, H., Kraut, R., Hayashi, S., Kotaoka, Y. and Takeichi, M.** (1996). Zygotic
430 Drosophila E-cadherin expression is required for processes of dynamic epithelial cell
431 rearrangement in the Drosophila embryo. *Genes Dev* **10**, 659-671.
432 **Wang, X., Zheng, M., Fei, F., Li, C., Du, J., Liu, K., Li, Y. and Zhang, S.** (2019). EMT-related
433 protein expression in polyploid giant cancer cells and their daughter cells with different
434 passages after triptolide treatment. *Med Oncol* **36**, 82.
435 **Weaver, L. N., Ma, T. and Drummond-Barbosa, D.** (2020). Analysis of Gal4 Expression
436 Patterns in Adult Drosophila Females. *G3 (Bethesda)* **10**, 4147-4158.
437 **Woods, D. F., Hough, C., Peel, D., Callaini, G. and Bryant, P. J.** (1996). Dlg protein is
438 required for junction structure, cell polarity, and proliferation control in Drosophila
439 epithelia. *J Cell Biol* **134**, 1469-1482.

440

441 **Figure Legends**

442 **Figure 1: Induction of premature follicle cell endocycles.** (A) Drawing of an ovariole with
443 select stages of oogenesis and follicle cell cycle transitions indicated below. Follicle cells are
444 pink. Above is the experimental timeline in relationship to the timing of egg chamber
445 maturation. (B-C′) DAPI staining and immunolabeling against E-cadherin in control (B, B′) and
446 Rux-expressing stage 10B egg chambers (C, C′); scale bar = 30 μm. (D) Quantification of DNA
447 Content (C) in control and Rux-expressing stage 10B egg chambers.; ****p < 0.0001; n = 85
448 nuclei in control and n = 104 nuclei in *UAS-Rux* across four biological replicates. (E)
449 Quantification of number of DAPI-labeled nuclei in control and Rux-expressing stage 10B egg
450 chambers; ****p < 0.0001; n = 12 egg chambers in both across four biological replicates.

451 **Figure 2: Premature endocycling compromises egg quality and female fertility.** (A-D)
452 Differential interference contrast images of control (A, C) and Rux-expressing (B, D) stage 10B
453 egg chambers after one (A, B) or two (C, D) days of incubation at 29°C; scale bar = 100 μm.
454 (E) Quantification of oocyte area in control and Rux-expressing stage 10 egg chambers.; *p <
455 0.05; for day one, n = 13 oocytes for control and n = 15 oocytes for UAS-*Rux* across three
456 biological replicates; for day 2, n = 20 oocytes for control and n = 24 oocytes for UAS-*Rux*
457 across five biological replicates. (F) Quantification of nurse cell compartment length; **p =
458 0.0021, ***p = 0.0002, ****p < 0.0001. For day 1, n = 20 egg chambers for control and UAS-
459 *Rux* across three biological replicates; for day 2, n = 27 egg chambers for control and n = 30
460 egg chambers for *UAS-Rux* across five biological replicates. (G-J′) DAPI staining and EdU
461 labeling of DNA replication in control (G, I, I′) and Rux-expressing (H, J, J′) stage 10B egg
462 chambers after one (G, H) or two (I-J′) days of incubation at 29°C; scale bar = 25 μm (G-I, J) or
463 10 μm (I′, J′). (K) Quantification of percent stage 10B egg chambers that had follicle cells
464 exhibiting pan-nuclear EdU labeling in control and Rux-expressing ovaries. ***p = 0.0003; n =
465 26 egg chambers for control and n = 19 egg chambers for *UAS-Rux* across three biological
466 replicates. (L-O) Brightfield images of eggs laid by control (L, N) and Rux-expressing females
467 (M, O) after one (L, M) or two (N, O) days of incubation at 29°C; scale bar = 200 μm.
468 Quantification of percent of eggs with thin shells (P) and hatch rate (Q) across three biological
469 replicates.

470 **Figure 3: Premature endocycling disrupts follicular epithelial structure.** (A-D″) DAPI
471 staining and immunolabeling against E-cadherin in control (A-A″, C-C″) or Rux-expressing (B-
472 B″, D-D″) early-stage egg chambers after one (A-B″) or two (C-D″) days of incubation at 29°C;
473 scale bar = 15 μm (A-D″). Stages (S) of oogenesis and germarium (G) are indicated. (E)
474 Quantification of DNA Content (C) in control and Rux-expressing stage 4 / 5 egg chambers
475 after two days of incubation at 29°C.; ****$p < 0.0001$; n = 25 nuclei for control and n = 15 nuclei
476 for *UAS-Rux* across three biological replicates.

477 **Figure 4: Premature endocycling inhibits border cell migration.** (A-B′) DAPI staining and
478 immunolabeling against E-cadherin in control (A, A′) and Rux-expressing (B, B′) egg chambers
479 after two days of incubation at 29°C; scale bar = 30 μm (A, B) or 15 μm (A′, B′). White arrows
480 indicate border cell clusters. White lines indicate extent of migration of border cell clusters, and
481 red lines indicate extent of migration of main body cells. (C) Quantification of border cell
482 migration during stage 9 from control and Rux-expressing females after two days of incubation
483 at 29°C across five biological replicates. Each dot represents one egg chamber with the
484 distance migrated by its main body and border cells plotted on the x- and y-axis, respectively.
485 (D- E‴) DAPI staining and immunolabeling against FasIII and E-cadherin in control (D-D‴) and
486 Rux-expressing (E-E‴) border cell clusters after two days of incubation at 29°C; scale bar = 10
487 μm.

Figure 1

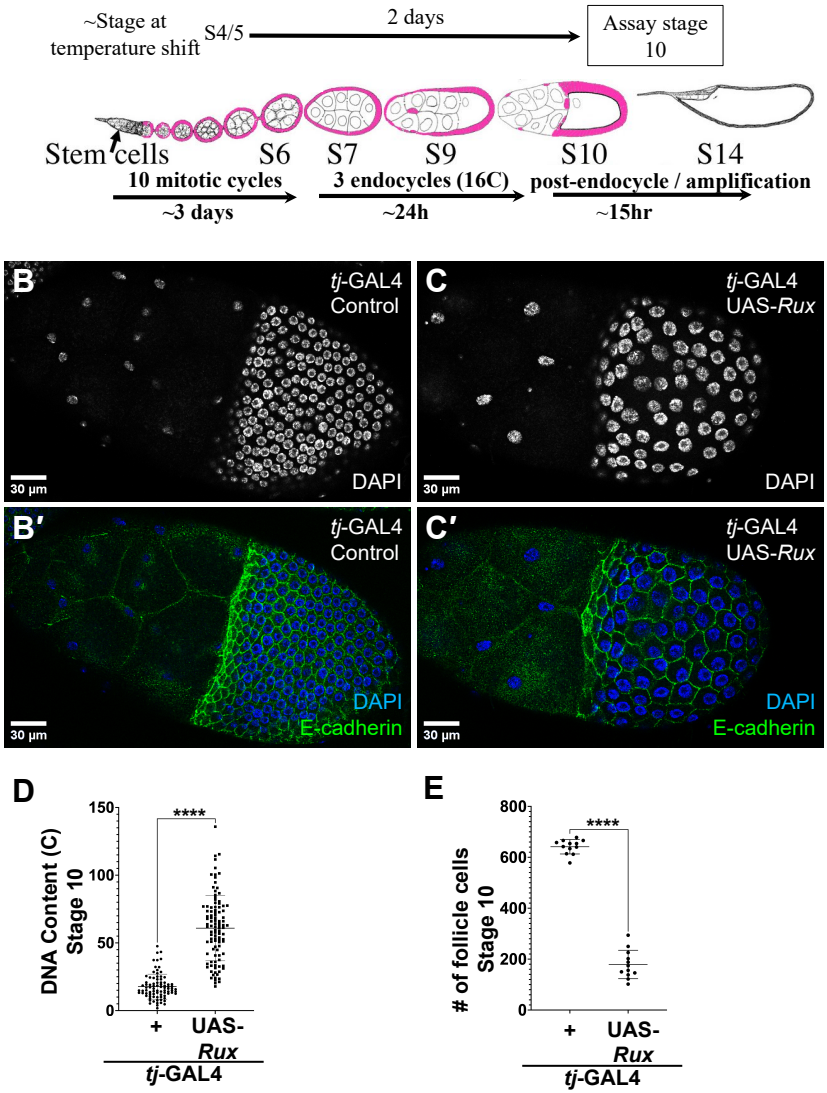
A
~Stage at temperature shift
S4/5
2 days
Assay stage 10
Stem cells
S6
S7
S9
S10
S14
10 mitotic cycles
~3 days
3 endocycles (16C)
~24h
post-endocycle / amplification
~15hr
B
tj-GAL4
Control
DAPI
30 µm
C
tj-GAL4
UAS-Rux
DAPI
30 µm
B′
tj-GAL4
Control
DAPI
E-cadherin
30 µm
C′
tj-GAL4
UAS-Rux
DAPI
E-cadherin
30 µm
D
DNA Content (C)
Stage 10
150
100
50
0
****
+
UAS-Rux
tj-GAL4
E
# of follicle cells
Stage 10
800
600
400
200
0
****
+
UAS-Rux
tj-GAL4

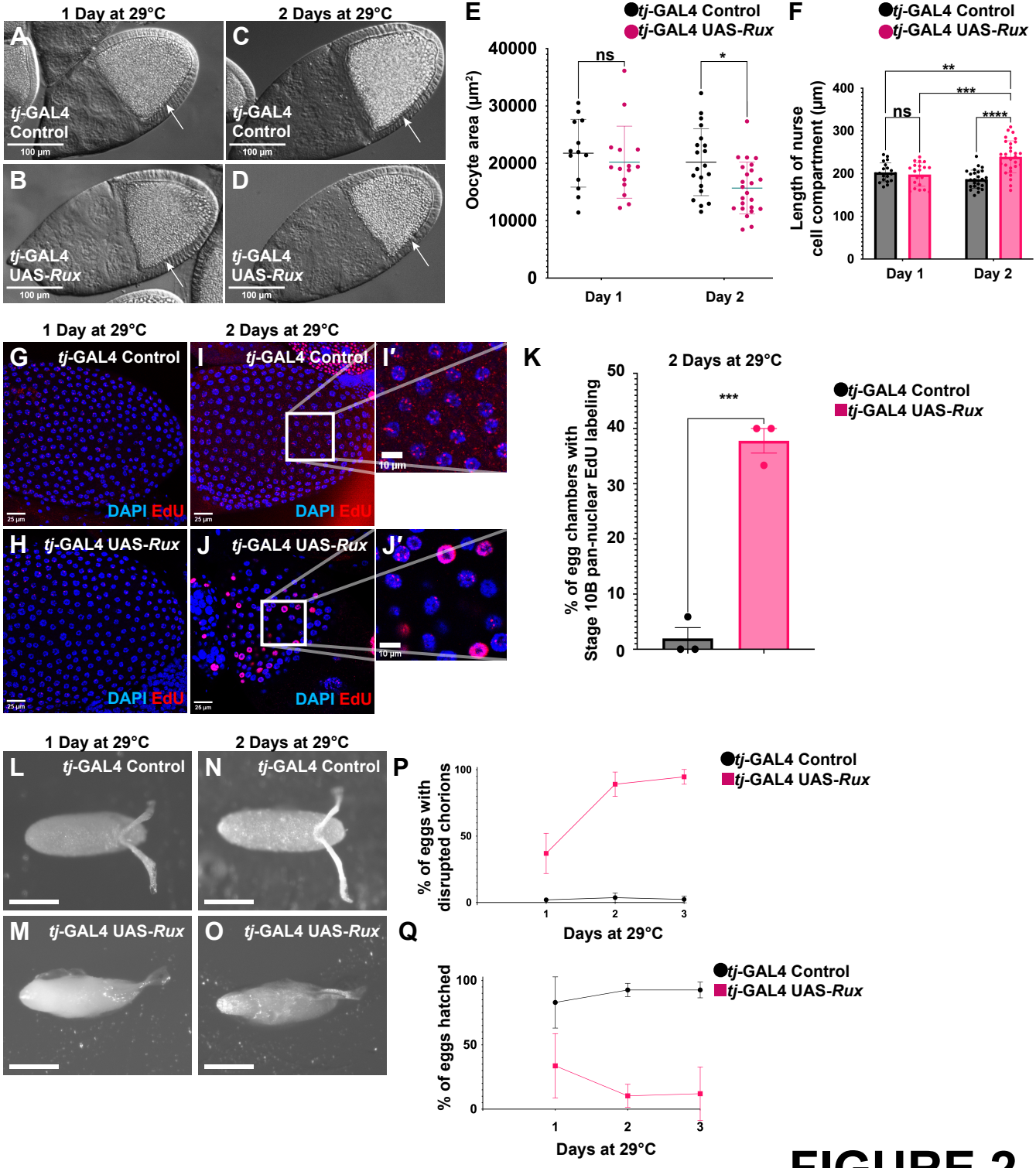
1 Day at 29°C
2 Days at 29°C
A
tj-GAL4 Control
100 µm
B
tj-GAL4 UAS-Rux
C
D
E
tj-GAL4 Control
tj-GAL4 UAS-Rux
Oocyte area (µm²)
ns
*
Day 1
Day 2
F
Length of nurse cell compartment (µm)
**
***
****
G
I
I'
H
J
J'
DAPI EdU
25 µm
10 µm
K
% of egg chambers with Stage 10B pan-nuclear EdU labeling
L
M
N
O
P
% of eggs with disrupted chorions
Days at 29°C
Q
% of eggs hatched

FIGURE 2

FIGURE 3

1 Day at 29°C

2 Days at 29°C

A *tj*-GAL4 Control
S2
S3/4
S5/6
S1
G
DAPI
15 µm

B *tj*-GAL4 UAS-*Rux*
S2
S3/4
DAPI
15 µm

C *tj*-GAL4 Control
S2
S3
S4
DAPI
15 µm

D *tj*-GAL4 UAS-*Rux*
S3/4
S5
DAPI
15 µm

A′ *tj*-GAL4 Control
S2
S3/4
S5/6
S1
G
E-cadherin
15 µm

B′ *tj*-GAL4 UAS-*Rux*
S2
S3/4
E-cadherin
15 µm

C′ *tj*-GAL4 Control
S2
S3
S4
E-cadherin
15 µm

D′ *tj*-GAL4 UAS-*Rux*
S3/4
S5
E-cadherin
15 µm

A″ *tj*-GAL4 Control
S2
S3/4
S5/6
S1
G
DAPI
E-cadherin
15 µm

B″ *tj*-GAL4 UAS-*Rux*
S2
S3/4
DAPI
E-cadherin
15 µm

C″ *tj*-GAL4 Control
S2
S3
S4
DAPI
E-cadherin
15 µm

D″ *tj*-GAL4 UAS-*Rux*
S3/4
S5
DAPI
E-cadherin
15 µm

E

2 Days at 29°C

DNA Content (C) Stage4/5

50
40
30
20
10
0

****

+

UAS-*Rux*

tj-GAL4

FIGURE 4

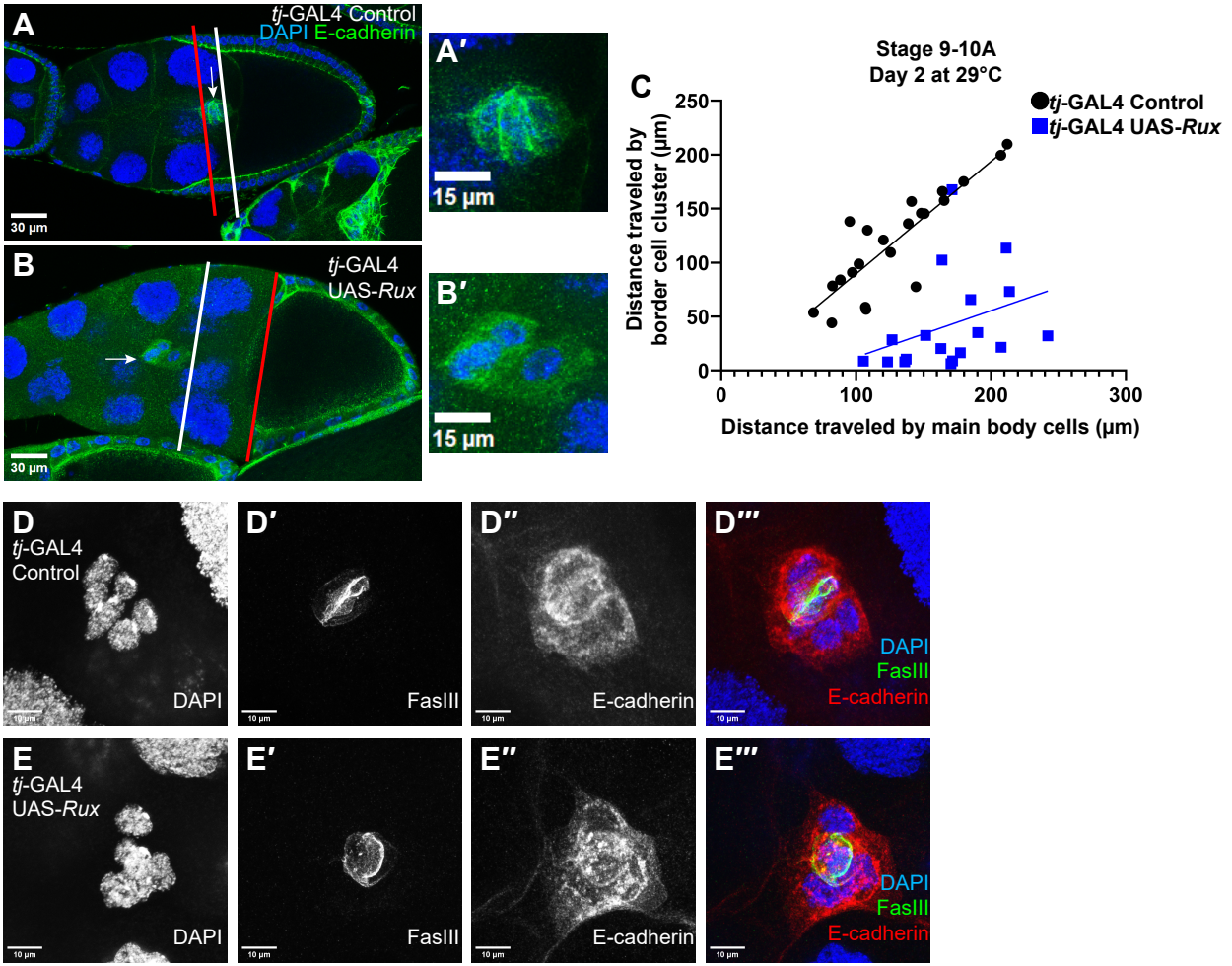
A
tj-GAL4 Control
DAPI E-cadherin
30 µm
A′
15 µm
B
tj-GAL4
UAS-Rux
30 µm
B′
15 µm
C
Stage 9-10A
Day 2 at 29°C
tj-GAL4 Control
tj-GAL4 UAS-Rux
Distance traveled by border cell cluster (µm)
Distance traveled by main body cells (µm)
0
50
100
150
200
250
0
100
200
300
D
tj-GAL4
Control
DAPI
D′
FasIII
D″
E-cadherin
D‴
DAPI
FasIII
E-cadherin
E
tj-GAL4
UAS-Rux
DAPI
E′
FasIII
E″
E-cadherin
E‴
DAPI
FasIII
E-cadherin